



Supplement of

Spatial and temporal variations in rockwall erosion rates derived from cosmogenic ^{10}Be in medial moraines at five valley glaciers around Pigne d’Arolla, Switzerland

Katharina Wetterauer and Dirk Scherler

Correspondence to: Katharina Wetterauer (katharina.wetterauer@gfz-potsdam.de)

The copyright of individual parts of the supplement might differ from the article licence.

S1 Supplementary Uncertainty Estimates on Boulder Velocities

We derived glacier surface velocities at Glacier du Brenay, Glacier de Cheilon, Glacier de Pièce, and Glacier de Tsijiore Nouve by manually tracing the displacement of medial moraine boulders across orthoimages between the years 1977 and 2020 (see Section 3.1.2). Uncertainties on these glacier surface velocities, respectively boulder velocities, mainly stem from three sources: (i) uncertainties in the positional accuracy for the orthoimages, (ii) uncertainties in the precision with which a boulder is identified and traced across successive orthoimages, and (iii) uncertainties in the length of the time period between two successive orthoimages. We discuss each of these points in the following paragraph.

(i) According to Swisstopo (2023), the positional accuracy for the orthoimages improves stepwise through time from ± 1 m (prior 1999) via ± 0.5 m (1998-2005) and ± 0.25 m (2005-2016) to ± 0.1 m (since 2017). (ii) The downglacier pathway and displacement of a medial moraine boulder is defined by tracing the boulder's centre as the reference point between the orthoimages. At all studied sites, the diameter of the tracked boulders typically varies between 2 and 4 m. We therefore approximate the relative uncertainty in identifying and tracing the boulder centre to no more than ± 0.5 m. (iii) The boulder velocity is given by the downglacier displacement divided by the time between two successive orthoimages. Unfortunately, exact acquisition dates for the orthoimages were unavailable, as the orthoimages are a mosaic of several individual black-and-white or colour aerial photographs from a particular year (Swisstopo, 2023). Therefore, we accounted for full years between the orthoimages. Nevertheless, the assumption that the orthoimages reflect a similar time during the summer season seems reasonable. At the studied sites, individual aerial photographs from the years 1977, 1983, 1988, 1995, 1999, and 2005 (available in the Swisstopo aerial imagery catalogue; Swisstopo, 2023) date to the beginning of September (± 1 month) and have presumably been used for the orthoimage composition, resulting in temporal deviations of ± 0.1 years.

Since uncertainties due to the positional accuracy vary for individual boulder tracking periods, we here provide as an example an average velocity uncertainty estimate for the four glaciers based on an early, a central, and a recent tracking period using Gaussian error propagation. For the early tracking period 1983-1988, the uncertainty for the average boulder displacement of ~ 100 m over 5 years is less than approximately 3% (yielding an average velocity and uncertainty of 20.0 ± 0.5 m yr⁻¹). For the central tracking period 1999-2005, the uncertainty for the average boulder displacement of ~ 70 m over 6 years is also less than approximately 3% (yielding an average velocity and uncertainty of 11.7 ± 0.3 m yr⁻¹). For the most recent tracking period 2017-2020, the uncertainty for the average boulder displacement of ~ 20 m over 3 years approximates less than 5% (yielding an average velocity and uncertainty of 6.7 ± 0.3 m yr⁻¹). Overall, these uncertainties are small and have no significant effect on the modelled sample ages.

S2 Supplementary Figures S1-S6

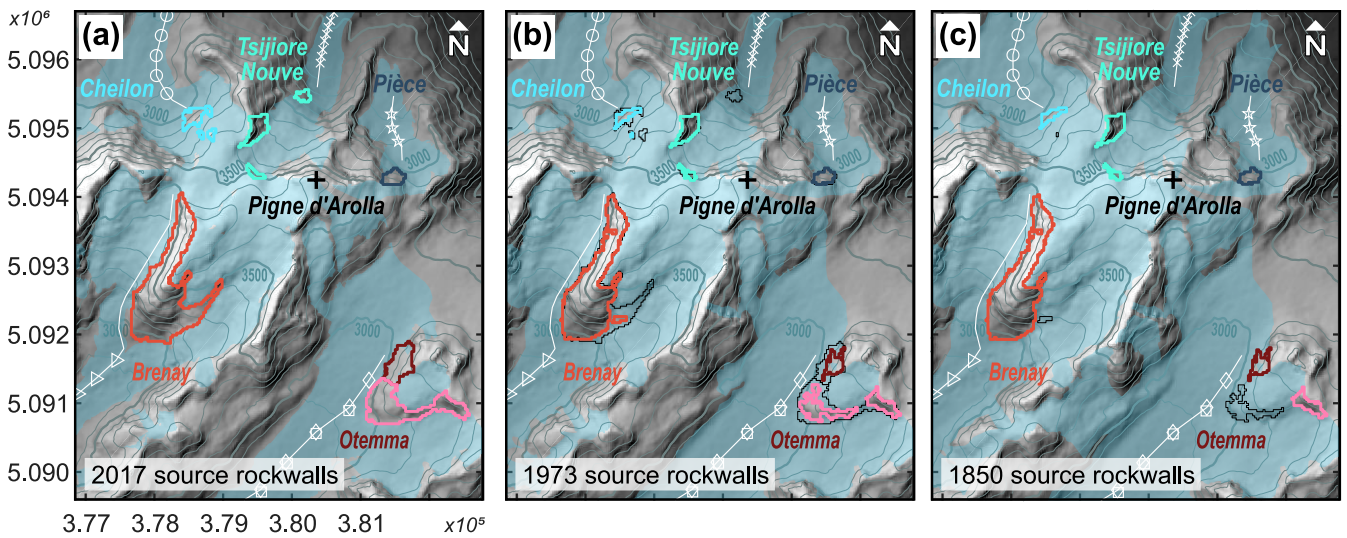


Figure S1: Hillshade images with elevation as greyscale (bright = high) outlining the studied ice-free source rockwalls around Pigne d'Arolla for the three time slices (a) 2017, (b) 1973, and (c) 1850. To visualize the temporal changes in ice cover across the debris source areas, source rockwall outlines of the year shown are coloured and underlain by the source rockwall outlines of the next younger time slice in black. 100 m contour lines are based on the recent DEM SRTM GL1 (NASA Shuttle Radar Topography Mission SRTM, 2013) and, therefore, on the glacier body itself only valid for the most recent time slice. For reference, the glacier extents (blue shade), medial moraine profiles (white lines), and 2019 sample locations (white symbols) of Glacier du Brenay, Glacier de Cheilon, Glacier d'Otemma, Glacier de Pièce, and Glacier de Tsijiore Nouvelle are indicated (glacier extents of 2016, 1973, and 1850 by Linsbauer et al., 2021; Müller et al., 1976; Maisch et al., 2000).

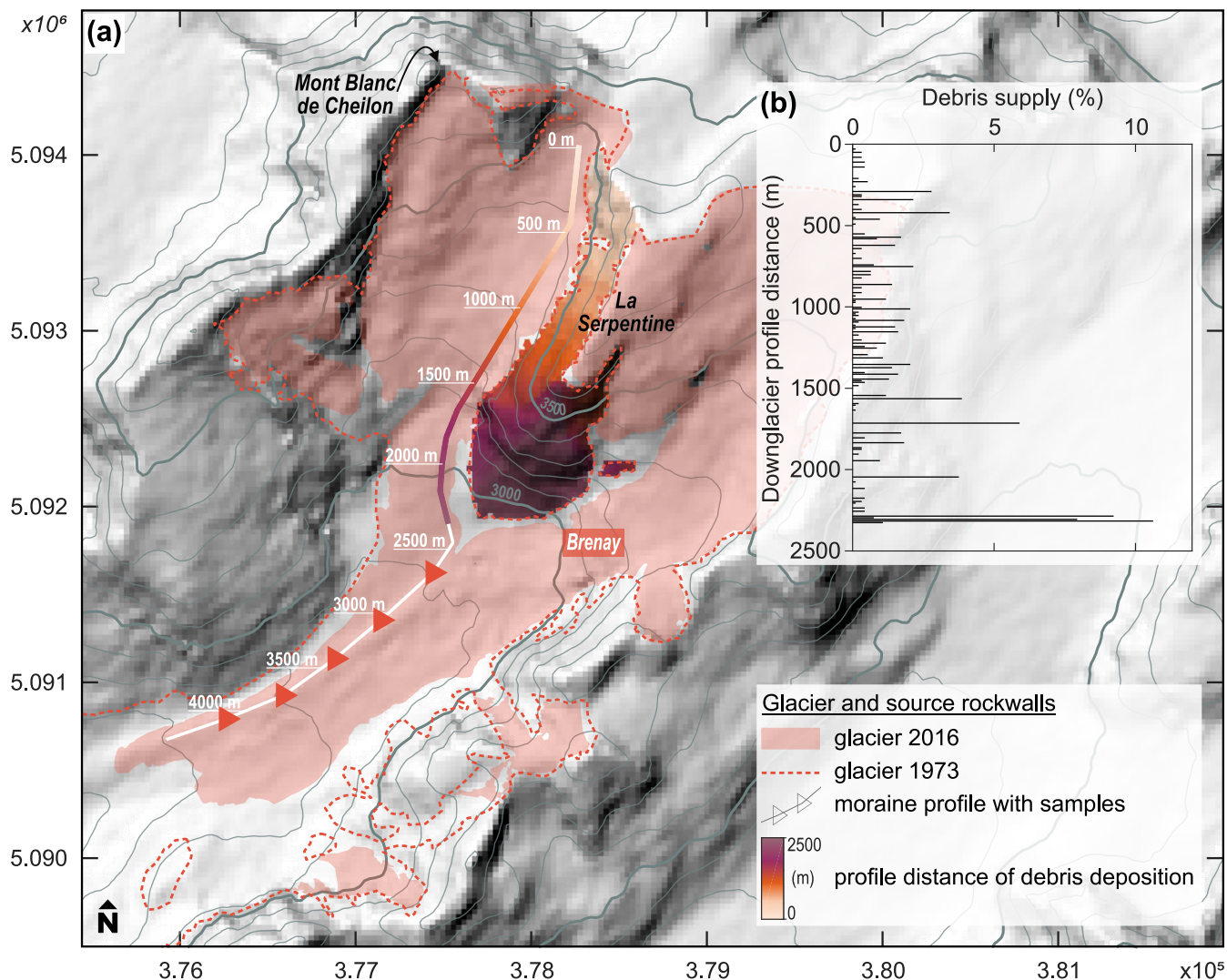


Figure S2: Weighted debris supply/deposition along the modelled medial moraine profile of Glacier du Brenay from ice-free source rockwalls of La Serpentine in 1973. (a) Hillshade image with elevation as greyscale (bright = high) showing that, due to the elongated nature of La Serpentine, debris deposition does not occur at a single confined location but along the first ~ 2.3 km of the modelled downglacier medial moraine profile. Therefore, at a sample location in 2019, trajectories of several debris particles will meet that were deposited at different profile distances and that experienced different transport times and exposures to cosmic radiation (see Fig. S3). The colour gradient along the downglacier profile and across the source rockwall area indicates at which downglacier profile distance a rockwall/DEM pixel supplies a debris particle, according to the flow directions of the steepest descent. Hillshade and 100 m contour lines are based on the DEM SRTM GL1 (NASA Shuttle Radar Topography Mission SRTM, 2013). For reference, the 2016 and 1973 glacier extents, the medial moraine profile with downglacier distances, and the 2019 sample locations are indicated (glacier extents by Linsbauer et al., 2021; Müller et al., 1976). (b) Inset aligning to the downglacier profile in (a) and showing the percentage debris particle supply along the first ~ 2.3 km profile distance, weighted by the overlying rockwall area. Assuming a constant erosion rate across La Serpentine, debris supply/deposition is relatively higher where more rockwall area towers above the ice, and thus those trajectories are more represented when estimating an average sample age based on all modelled trajectories.

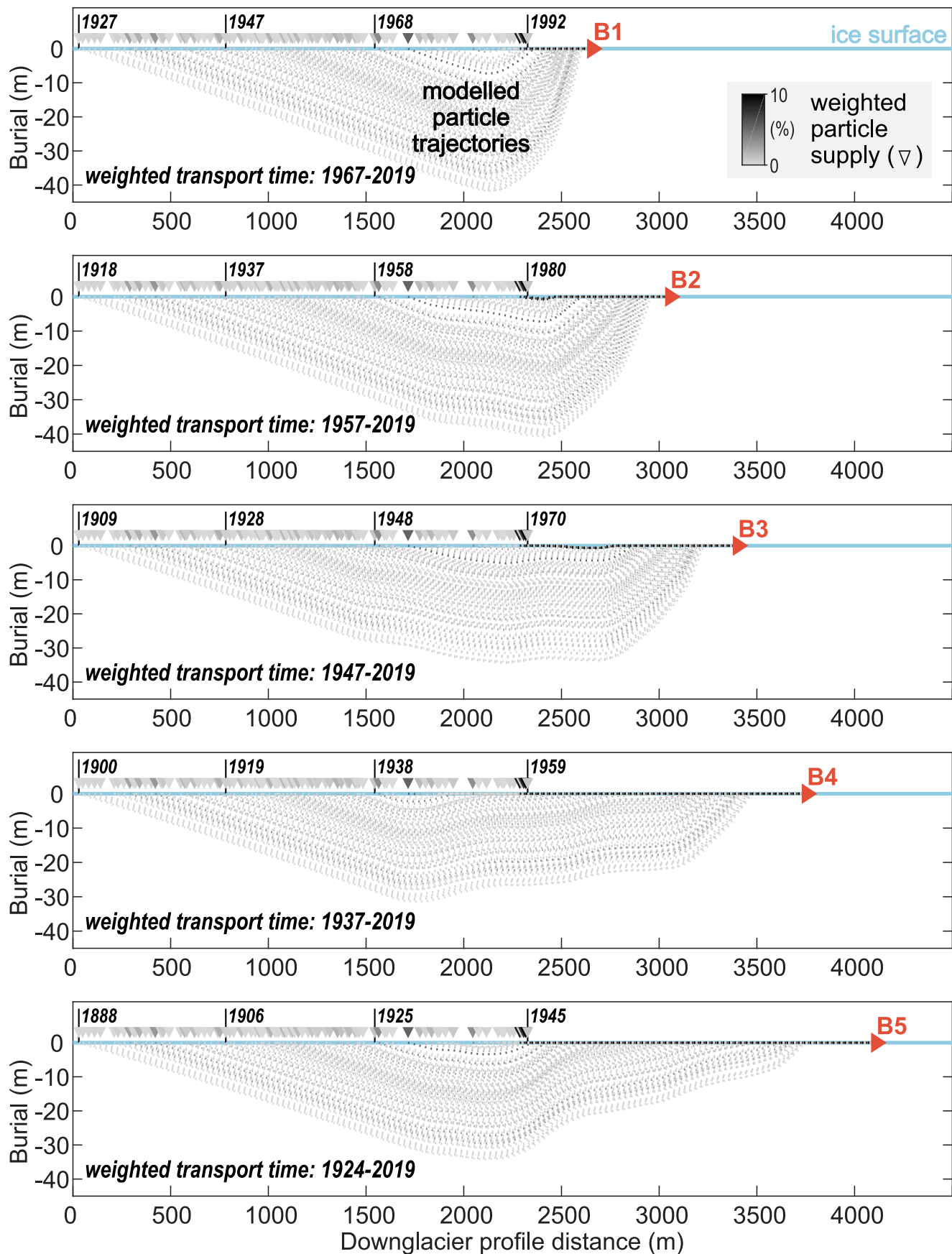
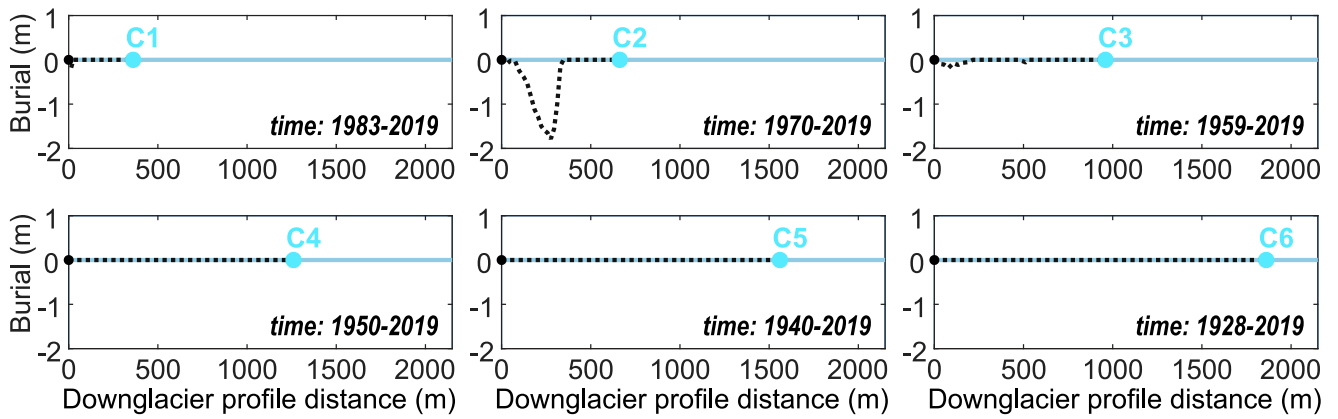
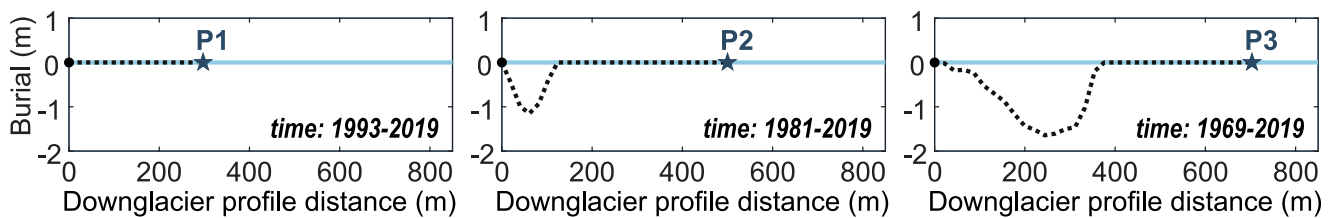


Figure S3: Modelled debris particle trajectories indicating the mode of downglacier particle transport from source rockwalls to sample locations B1-5 at Glacier du Brenay. Shown are all trajectories of particles deposited along the first ~2.3 km of the downglacier profile that arrive at the ice surface and downglacier distance of a sample's location in 2019. For reference, start years of four trajectories are given. The burial depth indicates whether a particle was transported within the ice (englacially; burial depth < 0 m) and shielded from cosmic radiation, or on the ice surface (supraglacially; burial depth = 0 m) and exposed to cosmic radiation. Graded colours indicate the percentage debris particle supply along the first ~2.3 km profile distance (see also Fig. S2b) and the weight of its corresponding trajectory, used to estimate a weighted time of downglacier particle transport.

(a) Cheilon



(b) Pièce



(c) Tsijiore Nouvelle

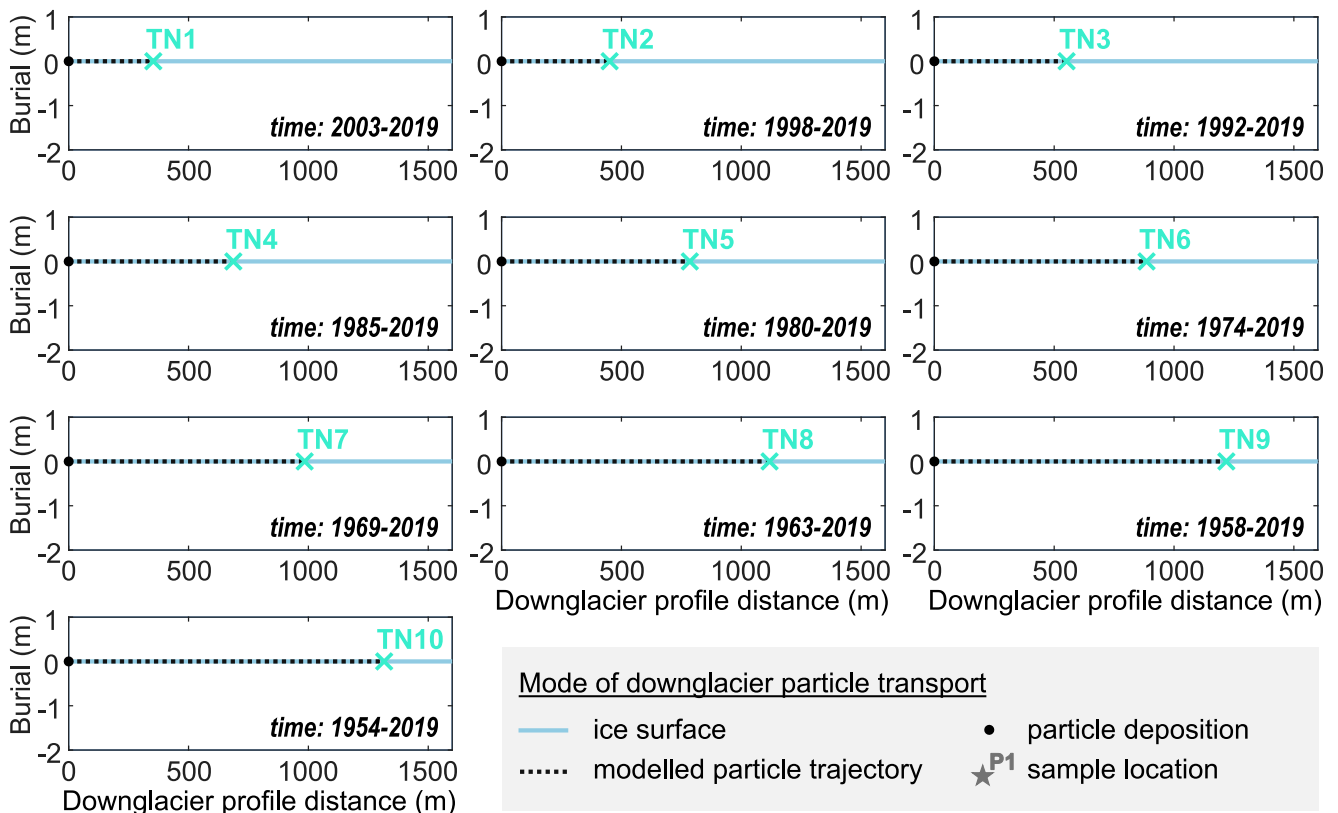


Figure S4: Modelled debris particle trajectories indicating the mode of downglacier particle transport from source rockwalls to sample locations at (a) Glacier de Cheilon, (b) Glacier de Pièce, and (c) Glacier de Tsijiore Nouvelle. Note that each graph stands for an individual sample. Shown is the burial depth of particles, which indicates whether a particle was transported within the ice (englacially; burial depth < 0 m) and shielded from cosmic radiation, or on the ice surface (supraglacially; burial depth = 0 m) and exposed to cosmic radiation. A particle's transport begins at the ice surface and profile head at the time as indicated and ends at the ice surface and downglacier distance of a sample's location in 2019.

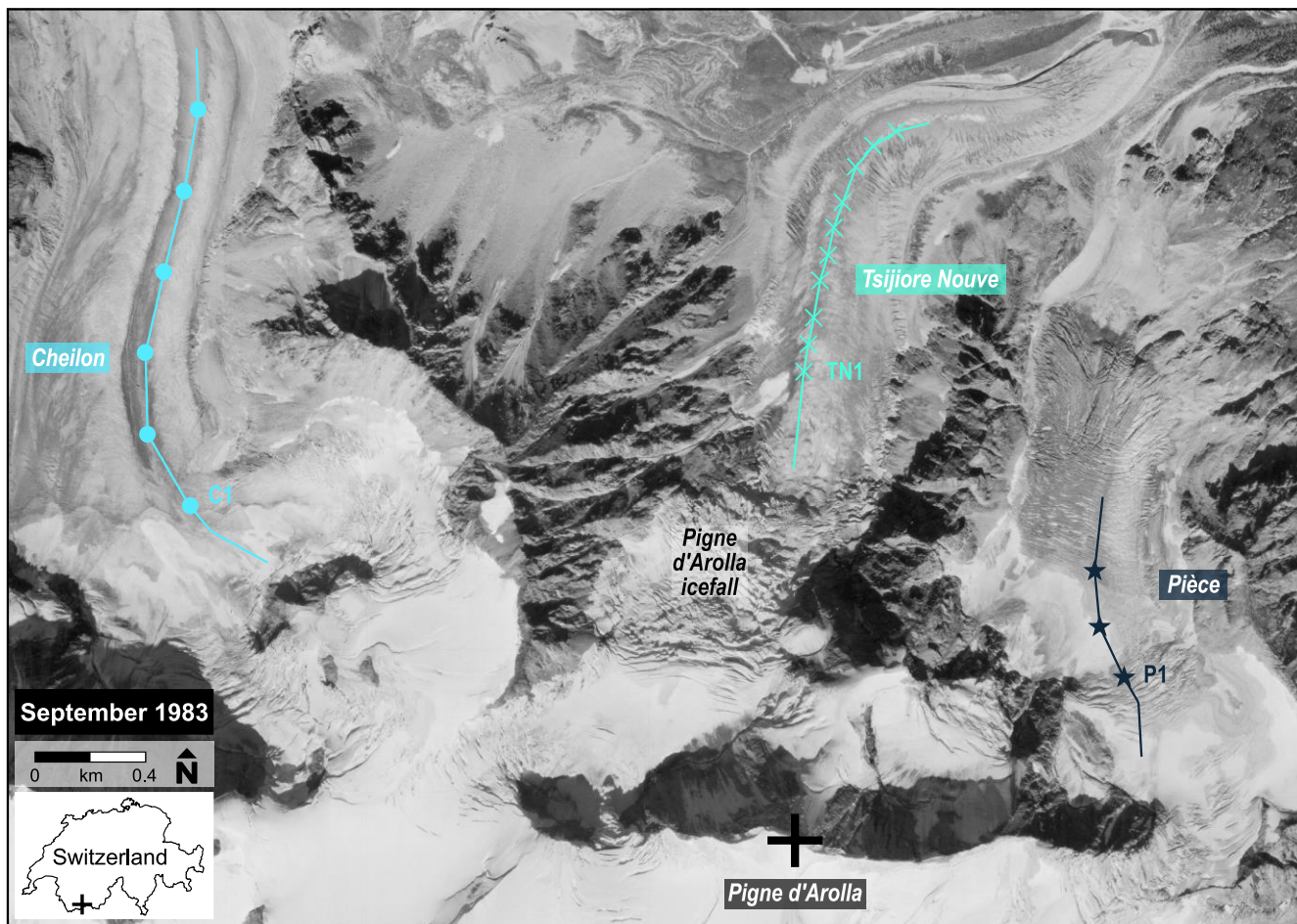


Figure S5: Orthoimage from 1983 indicating englacial debris transport close to the source rockwalls of Glacier de Cheilon and Glacier de Pièce as well as close to the base of the Pigne d'Arolla icefall at Glacier de Tsjiore Nouve. For reference, the respective medial moraine profiles and 2019 sample locations are indicated. The image excerpt is based on aerial images taken in September 1983 (orthoimage by Swisstopo, 2023).

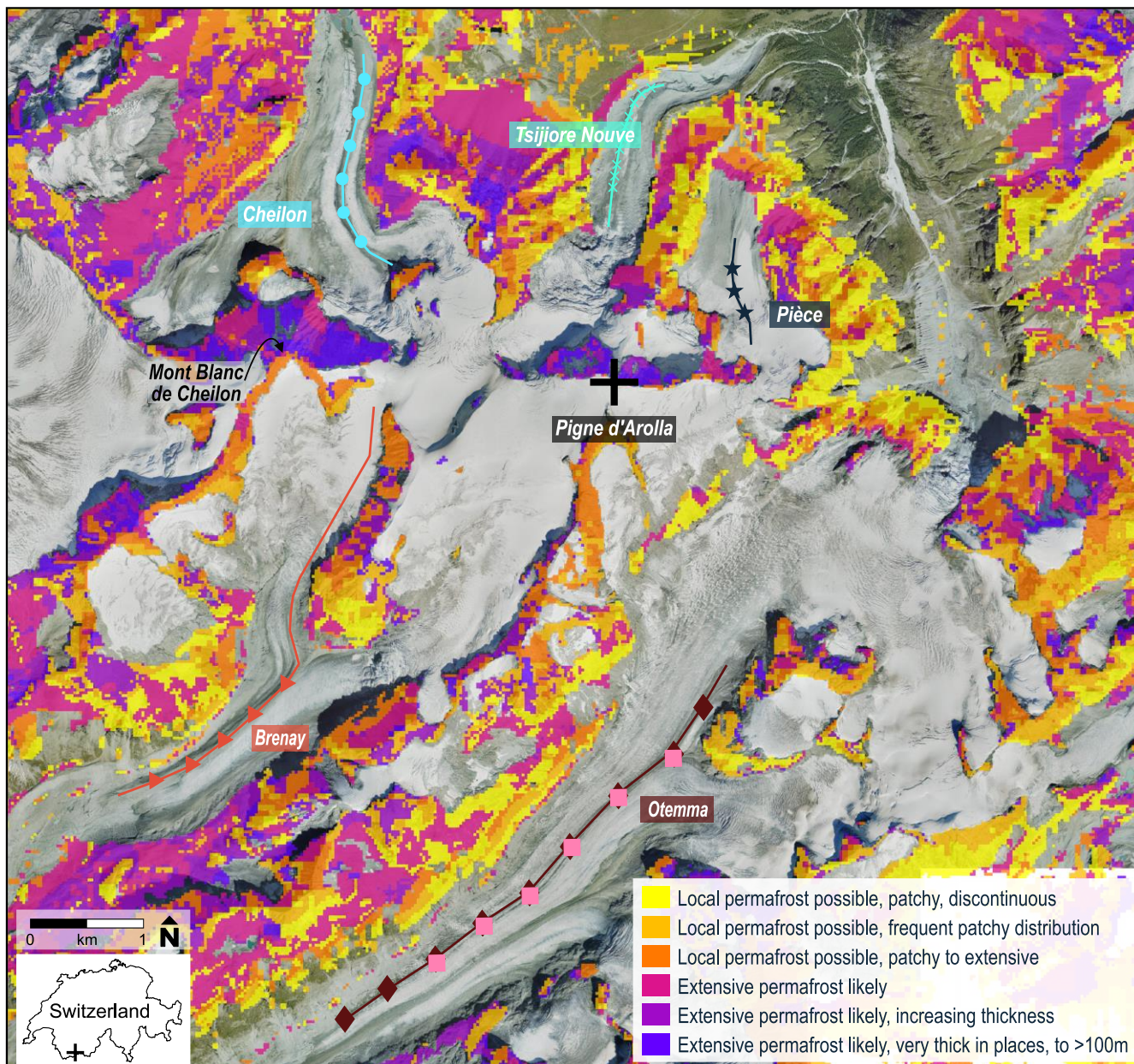


Figure S6: Permafrost distribution map showing the potential zone of modelled mountain permafrost across ice-free rockwalls and slopes in the area around Pigne d’Arolla. For reference, the respective medial moraine profiles and 2019 sample locations of Glacier du Brenay, Glacier de Cheilon, Glacier d’Otemma, Glacier de Pièce, and Glacier de Tsijiore Nouve are indicated. Note the extensive permafrost occurrence at the north faces of the east-west trending ridgeline between Pigne d’Arolla and Mont Blanc de Cheilon compared to the patchier permafrost occurrence to the south (potential permafrost distribution map by BAFU, 2005; orthoimage by Swisstopo, 2023).

S3 Supplementary Table S1

Table S1: Comparison of model results for downglacier debris particle transport at Glacier du Brenay, Glacier de Cheilon, Glacier de Pièce, and Glacier de Tsijiore Nouve using different glacier surface velocity projections into the past for which we lack boulder tracking data. Listed are the sample ages, the additional ^{10}Be accumulation ($[^{10}\text{Be}]_{\text{transport}}$), and the transport-corrected apparent rockwall erosion rates based on (1) the velocity projections used in the study, as well as (2) half and (3) twice the velocity assumptions made. Note that the age estimates for the slower/faster glacier surface velocities largely differ by <5 years, except for few samples at Glacier de Cheilon where age differences with up to 14 years are still relatively small and do not affect our findings. The data were computed using the simple 1D particle trajectory model by Wetterauer et al. (2022b) and, except for the glacier surface velocities, settings/calculations were kept as described in the study.

Sample	Past velocity projections used			1/2× past velocity projections			2× past velocity projections		
	Age (yrs)	$[^{10}\text{Be}]_{\text{transport}} \times 10^3$ (atoms g^{-1})	App. erosion rate (transport-corr.) (mm yr^{-1})	Age (yrs)	$[^{10}\text{Be}]_{\text{transport}} \times 10^3$ (atoms g^{-1})	App. erosion rate (transport-corr.) (mm yr^{-1})	Age (yrs)	$[^{10}\text{Be}]_{\text{transport}} \times 10^3$ (atoms g^{-1})	App. erosion rate (transport-corr.) (mm yr^{-1})
<i>Glacier du Brenay</i>									
B1	52	0.7	1.0	53	0.7	1.0	52	0.7	1.0
B2	63	0.9	0.7	63	0.8	0.7	62	0.9	0.7
B3	72	1.1	0.7	73	1.1	0.7	70	1.1	0.7
B4	83	1.5	0.8	84	1.5	0.8	80	1.6	0.8
B5	96	1.9	0.7	98	1.9	0.7	92	1.9	0.7
<i>Glacier de Cheilon</i>									
C1	36	1.0	5.1	36	1.0	5.1	36	1.0	5.1
C2	50	1.3	8.9	51	1.3	9.1	48	1.2	8.6
C3	61	1.7	4.5	65	1.8	4.7	55	1.6	4.4
C4	70	2.0	7.6	77	2.2	8.3	62	1.8	7.0
C5	80	2.3	36.7	90	2.5	87.5	70	2.0	23.2
C6	92	2.6	10.0	105	2.6	10.3	78	2.2	8.2
<i>Glacier de Pièce</i>									
P1	27	0.8	5.5	27	0.8	5.5	27	0.8	5.5
P2	39	1.0	5.9	39	1.0	5.9	39	1.0	5.9
P3	50	1.2	7.6	51	1.3	7.7	49	1.2	7.4
<i>Glacier de Tsijiore Nouve</i>									
TN1	16	0.4	10.6	16	0.4	10.6	16	0.4	10.6
TN2	21	0.5	12.7	21	0.5	12.7	21	0.5	12.7
TN3	27	0.6	18.7	27	0.6	18.7	27	0.6	18.7
TN4	34	0.8	15.6	34	0.8	15.6	34	0.8	15.6
TN5	40	0.9	21.3	40	0.9	21.3	40	0.9	21.3
TN6	45	1.0	7.4	45	1.0	7.4	45	1.0	7.4
TN7	50	1.1	15.1	50	1.1	15.1	50	1.1	15.1
TN8	56	1.3	9.3	56	1.3	9.3	56	1.3	9.3
TN9	61	1.4	34.5	61	1.4	34.5	60	1.4	33.2
TN10	65	1.5	18.9	66	1.5	19.3	65	1.4	18.7

S4 References

Bundesamt für Umwelt (BAFU): Hinweiskarte der potenziellen Permafrostverbreitung, <https://map.geo.admin.ch> (last access: 14 November 2022), 2005.

Linsbauer, A., Huss, M., Hodel, E., Bauder, A., Fischer, M., Weidmann, Y., Bärtschi, H., and Schmassmann, E.: The new Swiss Glacier Inventory SGI2016: from a topographical to a glaciological dataset, *Front. Earth Sci.*, 9, 1-22, <https://doi.org/10.3389/feart.2021.704189>, 2021.

Maisch, M., Wipf, A., Denneler, B., Battaglia, J., and Benz, C.: Die Gletscher der Schweizer Alpen: Gletscherhochstand 1850, Aktuelle Vergletscherung, Gletscherschwund-Szenarien, (Schlussbericht NFP 31), 2. Auflage. vdf Hochschulverlag an der ETH Zürich, Glacier Inventory 1850 [data set], <https://www.glamos.ch/en/downloads#inventories/B36-26> (last access: 19 June 2020), 2000.

Müller, F., Caflisch, T., and Müller, G.: Firn und Eis der Schweizer Alpen (Gletscherinventar), Publ. Nr. 57/57a. Geographisches Institut, ETH Zürich, 2 Vols., Glacier Inventory 1973 [data set], <https://www.glamos.ch/en/downloads#inventories/B36-26> (last access: 19 June 2020), 1976.

NASA Shuttle Radar Topography Mission SRTM: Shuttle Radar Topography Mission (SRTM) Global, OpenTopography [data set], <https://doi.org/10.5069/G9445JDF>, 2013.

Swisstopo: Federal Office of Topography Swisstopo, <https://map.geo.admin.ch>, last access: 25 May 2023.

Wetterauer, K., Scherler, D., Anderson, L.S., and Wittmann, H.: Sample and modelling data for cosmogenic ^{10}Be in medial moraine debris of Glacier d'Otemma, Switzerland, GFZ Data Services [data set], <https://doi.org/10.5880/GFZ.3.3.2021.007>, 2022b.